doi:10.1016/j.jmb.2012.07.006 J. Mol. Biol. (2012) 423, 198–216

Contents lists available at www.sciencedirect.com

Journal of Molecular Biology

journal homepage: http://ees.elsevier.com.jmb

The Role of Counterion Valence and Size in GAAA Tetraloop–Receptor Docking/Undocking Kinetics

Julie L. Fiore[1,2], Erik D. Holmstrom[1,2], Larry R. Fiegland[1], Jose H. Hodak[1] and David J. Nesbitt[1,2*]

[1]*JILA, National Institute of Standards and Technology and University of Colorado, Boulder, CO 80309, USA*
[2]*Department of Chemistry and Biochemistry, University of Colorado, Boulder, CO 80309, USA*

Received 15 May 2012; received in revised form 2 July 2012; accepted 3 July 2012
Available online 14 July 2012

Edited by D. E. Draper

Keywords:
RNA folding;
ions;
counterion condensation;
single-molecule FRET;
tetraloop–receptor

For RNA to fold into compact, ordered structures, it must overcome electrostatic repulsion between negatively charged phosphate groups by counterion recruitment. A physical understanding of the counterion-assisted folding process requires addressing how cations kinetically and thermodynamically control the folding equilibrium for each tertiary interaction in a full-length RNA. In this work, single-molecule FRET (*f*luorescence *r*esonance *e*nergy *t*ransfer) techniques are exploited to isolate and explore the cation-concentration-dependent kinetics for formation of a ubiquitous RNA tertiary interaction, that is, the docking/undocking of a GAAA tetraloop with its 11-nt receptor. Rate constants for docking (k_{dock}) and undocking (k_{undock}) are obtained as a function of cation concentration, size, and valence, specifically for the series Na^+, K^+, Mg^{2+}, Ca^{2+}, $Co(NH_3)_6^{3+}$, and spermidine^{3+}. Increasing cation concentration *accelerates* k_{dock} *dramatically* but achieves only a *slight decrease* in k_{undock}. These results can be kinetically modeled using parallel cation-*dependent* and cation-*independent* docking pathways, which allows for isolation of the folding kinetics from the interaction energetics of the cations with the undocked and docked states, respectively. This analysis reveals a preferential interaction of the cations with the transition state and docked state as compared to the undocked RNA, with the ion–RNA interaction strength growing with cation valence. However, the corresponding *number* of cations that are taken up by the RNA upon folding *decreases* with charge density of the cation. The only exception to these behaviors is spermidine^{3+}, whose weaker influence on the docking equilibria with respect to $Co(NH_3)_6^{3+}$ can be ascribed to steric effects preventing complete neutralization of the RNA phosphate groups.

Published by Elsevier Ltd.

Introduction

The ability of RNA molecules to assemble into compact, functional structures depends explicitly on neutralization of the negatively charged phosphate backbone by counter-cations.[1,2] The intracellular environment is composed of a wide variety of cations that can promote folding, for example, K^+ and Mg^{2+} are present in concentrations of ~150 mM and ~0.5–1 mM, respectively.[3–5] Organic cations, such as polyamines, are also abundant and implicated in a number of cellular folding processes.[6–8] Metal cations can interact with RNA through both specific coordination and nonspecific delocalized interactions, and thus, the relative efficacy of monovalent *versus* multivalent ions in aiding RNA folding is only beginning to be understood.[1,2,9–17] The most common type of RNA–ion interactions are

*Corresponding author. E-mail address: djn@jila.colorado.edu.

Abbreviations used: NLPB, nonlinear Poisson–Boltzmann; EDTA, ethylenediaminetetraacetic acid.

0022-2836/$ - see front matter. Published by Elsevier Ltd.

nonspecific and delocalized, that is, interactions with "diffuse", fully hydrated, mobile yet still localized ("condensed") cations.[14] Polyamine interactions with nucleic acids are also predominantly nonspecific and electrostatic.[18–21] Unfortunately, a truly quantitative, first principles' prediction of the dependence of RNA tertiary folding on cation concentration is challenging due to the nonperiodically varying electrostatic potential along an irregular RNA structure.[8] Though much progress has been made using nonlinear Poisson–Boltzmann (NLPB) theory to describe nucleic acid electrostatic potentials and the corresponding spatial distributions of cations,[22–25] these models still fail to accurately predict the "ion atmosphere" for multivalent cations around even well-defined DNA helices.[22,26] Clear theoretical deficiencies are also noted when using NLPB to characterize the role of multivalent ions in nucleic acid folding transitions,[26,27] necessitating treatments that consider ion–ion correlation effects (e.g., the tightly bound ion model) to quantify salt contributions to RNA folding.[28,29] Furthermore, current theories are still limited in describing the folding dependence on cation size.[22,30–32] For all of the above reasons, simpler models, such as Manning counterion condensation theory, have proven useful in describing the cation dependence of *Tetrahymena* ribozyme folding rates and equilibrium.[33,34] An even more complicated task is describing mixed cationic environments, which can lead to both cation competition and synergy.[35,36]

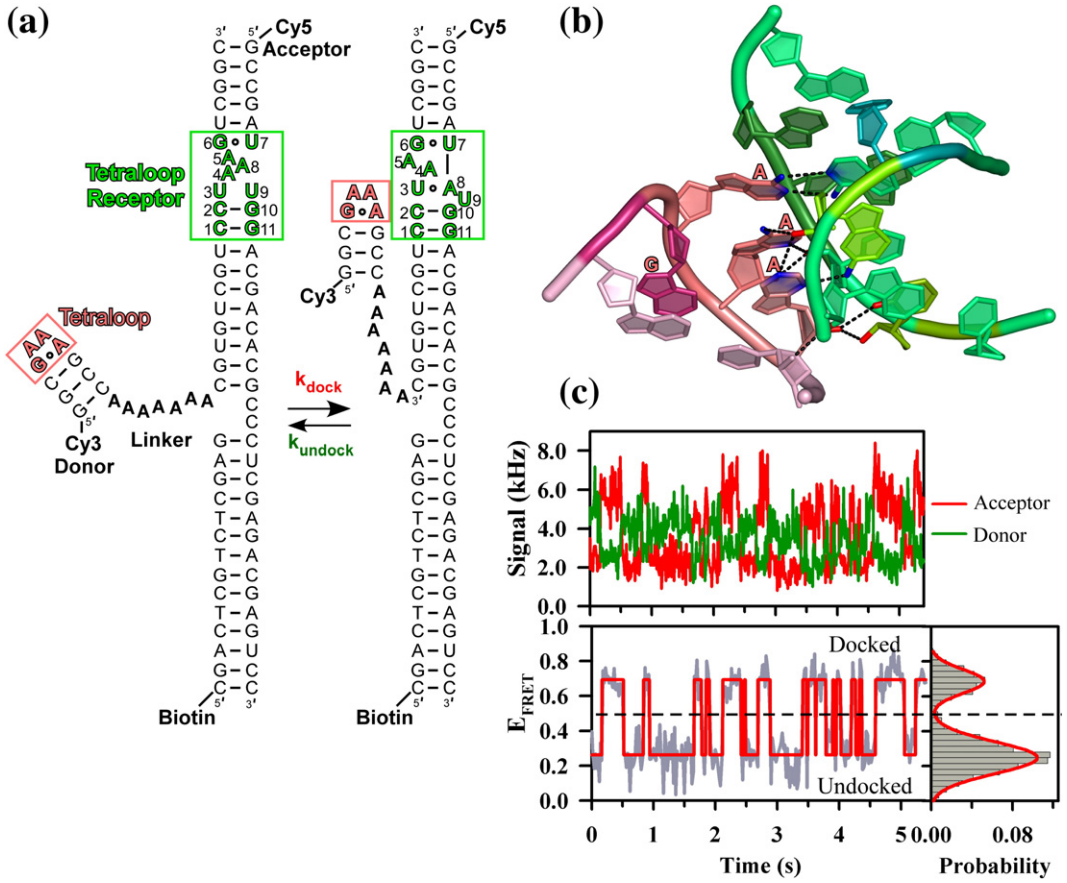

Fig. 1. GAAA tetraloop–receptor docking/undocking interaction. (a) Schematic of the observable folding transition in an RNA construct isolating the tetraloop–receptor interaction, characterized by rate constants k_{dock} and k_{undock}. Changes in FRET efficiency between Cy3 and Cy5 allow monitoring of GAAA tetraloop docking with the receptor. The RNA is immobilized on glass surfaces with biotin–streptavidin binding. (b) Structure of the GAAA tetraloop (AAA shown in salmon, G shown in magenta, and closing base pair shown in light pink) and its canonical 11-nt receptor (green) in the *Tetrahymena* ribozyme's P4–P6 domain. Ten hydrogen bonds form between the tetraloop and the receptor regions, shown as black broken lines. Blue, nitrogen; red, oxygen (hydrogens not shown) (Protein Data Bank ID 1HR2). (c) Monitoring tetraloop–receptor docking/undocking by FRET as seen by the anti-correlated donor and acceptor fluorescence signals and corresponding E_{FRET} (gray lines) trajectory with hidden Markov two-state fit shown in red. The probability distribution of the E_{FRET} traces reveals well-resolved docked and undocked states. The conditions shown are 100 mM KCl, 50 mM Hepes, and 0.1 mM EDTA at pH 7.5 and 21 °C.

Adding to these challenges is the fact that the structure of RNA is often quite *dynamic*, that is, with non-negligible rate constants for folding/unfolding and thus charge distributions necessarily varying as the molecule changes conformation.[1] Folding increases the negative charge density of RNA, strengthening RNA–ion interactions; as a result, even RNA nominally "at equilibrium" experiences a dynamic uptake/expulsion of counterions.[35,37,38] Thus, knowledge of the differential counterion affinity for native *versus* unfolded conformations is obviously critical to address cation-mediated folding. A further theoretical challenge in describing cation–RNA interactions is that the unfolded state exists as an ensemble of possible configurations, sampling of which can be altered by the local ion atmosphere.[39]

Though much work has been performed on the cation concentration dependence of *equilibrium* distributions, it is less well understood how cation-induced stabilization correlates with *kinetic rate constants* for RNA folding and unfolding. In principle, although accessible via stop-flow methods, counterion effects on folding/unfolding kinetics in RNA have been challenging to obtain from ensemble studies, which, to date, have precluded a mechanistic identification of the role of cations. In single-molecule FRET (*f*luorescence *r*esonance *e*nergy *t*ransfer) studies, on the other hand, folding and unfolding rates can be extracted under equilibrium conditions, based on how folding of a fluorescently labeled RNA changes dye-pair proximity. From the FRET efficiency, $E_{\mathrm{FRET}}(R) = R_0^6/(R_0^6 + R^6)$, this translates into readily measurable real-time changes in E_{FRET}, where R_0 is the Förster radius for 50% energy transfer probability and R is the inter-dye distance. Indeed, single-molecule FRET studies of RNA have revealed particularly rich [cation]-dependent folding kinetics. The RNA folding picture has been significantly advanced by the folding/unfolding kinetic studies of the hairpin ribozyme,[35,40,41] RNase P,[42] the *Tetrahymena* ribozyme,[43–45] three- and four-helix junctions,[46,47] and a group II intron.[48] Furthermore, single-molecule techniques have revealed that unique structural subpopulations may exist in the presence of different cations, for example, Ca^{2+} *versus* Mg^{2+}.[49]

RNA folding proceeds hierarchically, with a three-dimensional structure proceeding from association of well-defined secondary elements[17,50,51]; thus, tertiary interaction "motifs" have emerged as a common theme in RNA folding.[52,53] As a corollary, it is interesting to approach such a complex issue from a more reductionist perspective, that is, investigating the counterion-dependent kinetics for formation of an *isolated tertiary interaction*. Toward this end, we have explored the kinetics of the ubiquitous GAAA tetraloop–receptor tertiary interaction (Fig. 1a and b), which contributes to the proper folding and activity of a variety of structured RNAs, including group I and II introns and RNase P.[54–57] Also of background relevance is that both structures of the free and bound forms of the tetraloop and receptor have been determined.[11,58–60] The tetraloop is structurally unaltered by binding, but the receptor undergoes significant rearrangement.[11,58–60] The tetraloop–receptor interaction can form outside the context of large RNAs[60,61] and under a wide range of ionic conditions,[62] making it an ideal tertiary motif for study at the single-molecule level. To isolate this tertiary interaction, we have developed a single-molecule construct for characterization of intramolecular docking, based on a GAAA tetraloop with its 11-nt canonical receptor connected by an A_7 single-stranded linker (Fig. 1a). In previous ensemble FRET measurements, this tetraloop–receptor interaction has been shown to be enabled by many different cations.[63] Although such studies did reveal an equilibrium shift that favors docking with increasing cation concentration, they were not able to identify the kinetic origin of this shift. In contrast, single-molecule FRET studies of this construct have permitted the underlying kinetics to be studied, which reveal that *both* undocking and docking rate constants are affected by $[Mg^{2+}]$.[64] Moreover, recent calorimetric and single-molecule studies have elucidated fundamental differences in the underlying thermodynamics of the tetraloop–receptor interaction in monovalent *versus* divalent cationic environments,[65–67] highlighting the need to further understand the role of cation identity in RNA–ion interactions.

In the present work, we substantially expand our single-molecule FRET exploration of counterion effects on GAAA tetraloop–receptor folding/unfolding kinetics, with investigation of monovalents (Na^+ and K^+), divalents (Mg^{2+} and Ca^{2+}), and trivalents [$Co(NH_3)_6^{3+}$ and spermidine^{3+}] as a systematic function of cationic size and charge. Although the magnitude of the binding affinities differs by 3 orders of magnitude as a function of cation charge, the results can be simply summarized. Each of these ions affects the folding free-energy landscape remarkably similarly, by a combination of (i) dramatically increasing the docking rate constant, k_{dock}, while (ii) reducing the undocking rate constant, k_{undock}. Spermidine^{3+}, however, promotes folding to a lesser extent under saturating conditions than the other cations investigated. We find that cation *charge* provides the major distinction between the ion–RNA binding affinities. These observations are all consistent with a kinetic mechanism of RNA folding facilitated by counterion condensation. Furthermore, the origin of a cation-induced enhancement for RNA folding follows the same mechanism for each cation, that is, the overall thermodynamic stability of the docked form

($-\Delta G^{o}_{dock}$) *increases* more rapidly than the corresponding transition-state barrier free energy for docking ($\Delta G^{\ddagger}_{dock}$) *decreases*. Finally, a simple statistical mechanical analysis of the preferential interaction coefficient for RNA reveals that the number of cations taken up with folding changes dramatically as a function of cation identity and concentration.

Results

Tetraloop–receptor docking promoted by monovalent, divalent, and trivalent cations

Intramolecular docking of the GAAA tetraloop into the tetraloop–receptor (Fig. 1a and b) is monitored as a function of cationic conditions to investigate the importance of counterion valence and size for tertiary RNA folding. Specifically, we examine the effect of [Na^+], [K^+], [Mg^{2+}], [Ca^{2+}], [$Co(NH_3)_6^{3+}$], and [spermidine^{3+}] on the tetraloop–receptor docking/undocking kinetics. Tetraloop–receptor docking and undocking are monitored by single-molecule FRET, which reveals well-resolved docked/undocked states in real time (Fig. 1c).[64] At low monovalent concentration (100 mM KCl; Fig. 1c), the RNA spends the majority of its time undocked, with increased concentration of monovalent cation (e.g., 300 mM) systematically shifting the tetraloop–receptor equilibrium to favor docking (Fig. 2). Interestingly, a comparable distribution of docked/undocked states can be achieved under conditions with just 1 mM *divalent* or 0.1 mM *trivalent* cations, as shown in the E_{FRET} trajectories displayed in Fig. 2 [see Materials and Methods and Supplementary Information (Supplementary Text and Fig. S1) regarding experimental determination of E_{FRET}]. Thus, docking of the tetraloop and receptor appears to be effectively promoted by cations with a variety of sizes and valences and over a wide dynamic range of concentrations.

As apparent in these sample trajectories, the RNA constructs fluctuate between undocked and docked states (low E_{FRET} and high E_{FRET}, respectively), with distributions well described by a sum of Gaussians centered at $\langle E_{FRET}\rangle = 0.26 \pm 0.02$ and 0.69 ± 0.01, respectively. These mean FRET values are consistent both from cation to cation and for other ranges of concentration conditions observed, as well as with quantitative predictions of donor–acceptor distances anticipated from the RNA construct design.[36,64] Trajectories for Na^+ and K^+ ions reveal essentially indistinguishable FRET distributions at 300 mM, indicating no dependence on cation size among monovalents (Fig. 2). The FRET distributions for *divalent* Ca^{2+} and Mg^{2+} appear similar at 1 mM, though further analysis reveals a subtle difference between these cations (see the next section). Continuing this trend, differences are most apparent for the two *trivalent* ions investigated, with cobalt(III) hexamine achieving a considerably higher equilibrium constant for docking than spermidine^{3+} at 100 μM. In contrast to these smaller effects, however, the cation concentration necessary to promote docking is extremely dependent on ion valence. The data in Fig. 2 indicate a trend in the range of ion concentrations required for docking promotion characterized by [monovalent]>[divalents]>[trivalents], consistent with ensemble and freely diffusing single-molecule measurements but, here, obtained

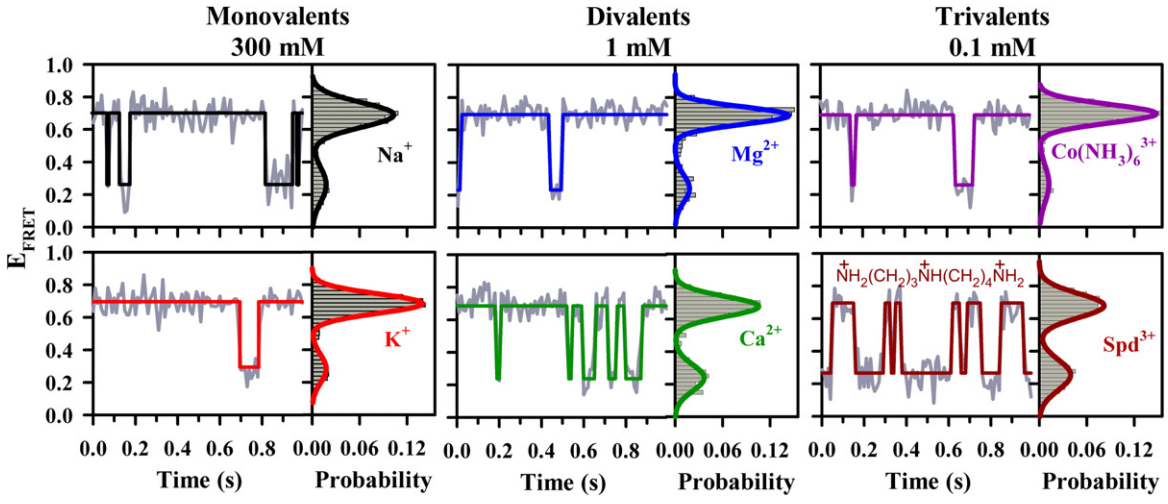

Fig. 2. Sample FRET efficiency trajectories and probability distributions for tetraloop–receptor docking/undocking in concentrations of 300 mM monovalent (Na^+ or K^+), 1 mM divalent (Mg^{2+} or Ca^{2+}), or 100 μM trivalent [$Co(NH_3)_6^{3+}$ or spermidine^{3+} (Spd^{3+})] concentrations. The RNA fluctuates between high and low E_{FRET} states. Data are shown in gray with hidden Markov fits overlaid in color. Positively charged amino groups are covalently linked by hydrocarbon chains in spermidine^{3+} (lower right panel).

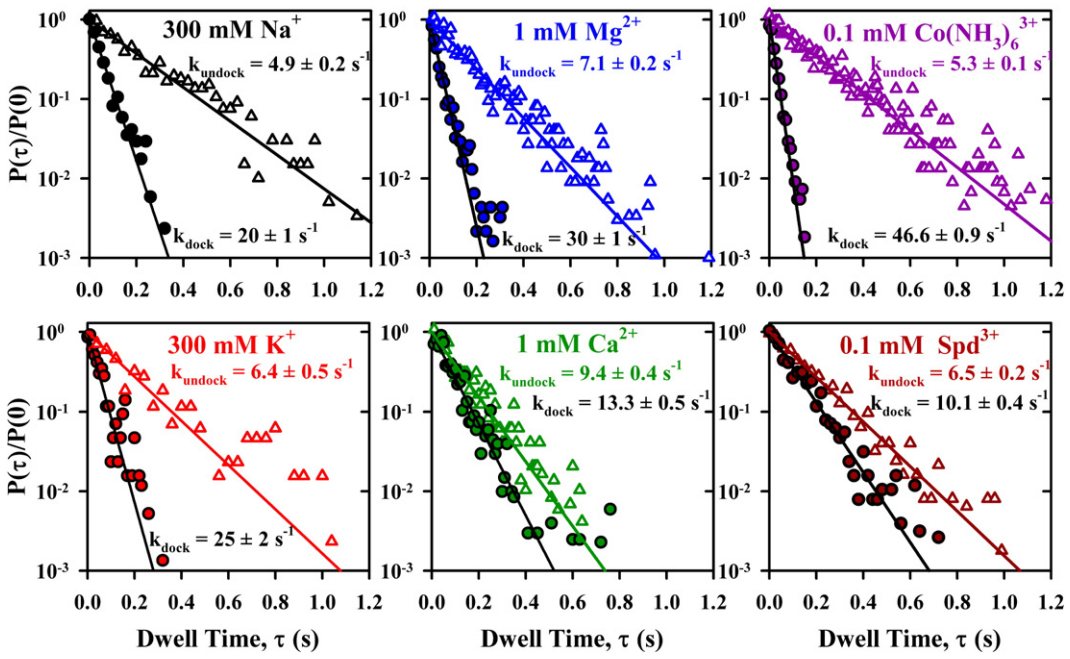

Fig. 3. Cumulative normalized probability densities for tetraloop–receptor dwell time (τ) in the docked (open triangles, △) and undocked (filled circles, ●) states at 300 mM monovalent (Na^+ and K^+), 1 mM divalent (Mg^{2+} and Ca^{2+}), and 100 μM trivalent [$Co(NH_3)_6^{3+}$ and spermidine^{3+} (Spd^{3+})] concentrations. Each probability density plot is compiled from >10 molecules and least squares fit to a single-exponential function, yielding the rate constants for docking (k_{dock}, black lines), undocking (k_{undock}, colored lines), and the corresponding uncertainties.

at the single-molecule kinetic level (bulk ensemble fluorometry data are shown for spermidine^{3+} in Supplementary Information and Fig. S2).[36,63]

Cation dependence of k_{dock} and k_{undock}

Although the equilibrium FRET distributions in Fig. 2 are already quite revealing, a much more quantitative comparison of the relative cation-induced stability can be obtained by extraction of the k_{dock} and k_{undock} rate constants for docking and undocking from the single-molecule trajectories. Sample probability densities for the dwell times in the undocked and docked states (see Materials and Methods) are shown in Fig. 3 for the same series of monovalent, divalent, and trivalent ions displayed in Fig. 2. These semi-log plots are linear over nearly 3 orders of magnitude, corresponding to a single-exponential decay of the dwell-time probabilities and consistent with a simple first-order kinetic process. Single-exponential fits of the probability densities from compilations of many molecules (typically ~10–30 molecules, comprising 200–2000 events) yield k_{dock} and k_{undock} from the undocked and docked dwell-time distributions, respectively. As anticipated from the E_{FRET} distributions (Fig. 2), these plots (Fig. 3) reveal that the rate constants are nearly indistinguishable for K^+ *versus* Na^+ at 300 mM, with subtle differences between 1 mM divalents (k_{dock} is 2.3±0.1-fold faster for Mg^{2+} *versus* Ca^{2+}) and larger differences for 100 μM trivalents [k_{dock} is 4.6±0.2-fold faster for $Co(NH_3)_6^{3+}$ *versus* sperimidine^{3+}].

The large dynamic range in these plots is rather remarkable (Fig. 3), spanning up to 3 orders of magnitude, and a tribute to the method for extraction of probability densities from the data. On more careful inspection, it is worth noting that such large dynamic range also permits subtle deviations from single-exponential behavior to be observed at very long event durations in each of the dwell-time distributions, as we previously described.[64] Such deviation from pure single-exponential behavior arises naturally from a more complex kinetic model framework.[64] However, the excellent linearity observed over 2 to 3 orders of magnitude indicates the kinetics to be overwhelmingly first order, with additional kinetic effects due to non-first-order behavior safely neglected in our analysis. Other than a minor subpopulation of molecules that lack docking/undocking events during a time trace (Materials and Methods),[64] significant molecule-to-molecule kinetic deviation has not been noted. This observation is important to emphasize because dynamic heterogeneity is commonly reported in single-molecule RNA folding studies.[35,40,41,43,68]

The titration results for first-order rate constants k_{dock} and k_{undock} on cation identity and concentration are summarized in Fig. 4 and reveal several

notable points. First of all, the relevant concentration axes differ dramatically with ionic charge, with 3 orders of magnitude higher monovalent than trivalent cation concentrations needed to achieve a given change in folding/unfolding rate constant. Second, these data do reveal a substantial similarity in shape, with (i) a steep *increase* in k_{dock} and (ii) a less dramatic but quite notable *decrease* in k_{undock} with increasing [cation]. Finally, both docking/undocking rate constants exhibit a clear saturation under high [cation] conditions, with asymptotic values corresponding to roughly a 12-fold *increase* in k_{dock} and a 3-fold *decrease* in k_{undock} for each combination of cation and charge state with the exception of spermidine^{3+}.

We note that the divalent and trivalent titrations are performed with 100 mM NaCl as a baseline because it (i) provides a physiologically relevant background ionic strength, (ii) more closely maintains conditions of constant ionic strength/activity conditions (due to excess Cl^- anion), and (iii) therefore enables cleaner interpretation of the multivalent cation effects on folding.[69] Furthermore, a 100-mM monovalent background permits electrostatic relaxation of any rigid helix secondary structure without contributing dramatically to tertiary structure formation.[36,70] The monovalent titrations, on the other hand, necessarily extend from a baseline buffer level (50 mM hemisodium Hepes) on upwards. As a result, the dynamic range of values for k_{dock} and k_{undock} are greatest for the monovalents (Fig. 4), with strong sigmoidal indications of ion cooperativity evident at the lowest monovalent concentrations. Unlike in the multivalent titrations, where ion thermodynamic activity ("effective concentration") increases proportionally to salt concentration, the effects of activity on the monovalent titrations must be considered. At >500 mM monovalent, the increase in activity with concentration is softened,[71] which slightly exaggerates the abruptness of the asymptotic saturation (Fig. 4). This effect is of minor consequence to the

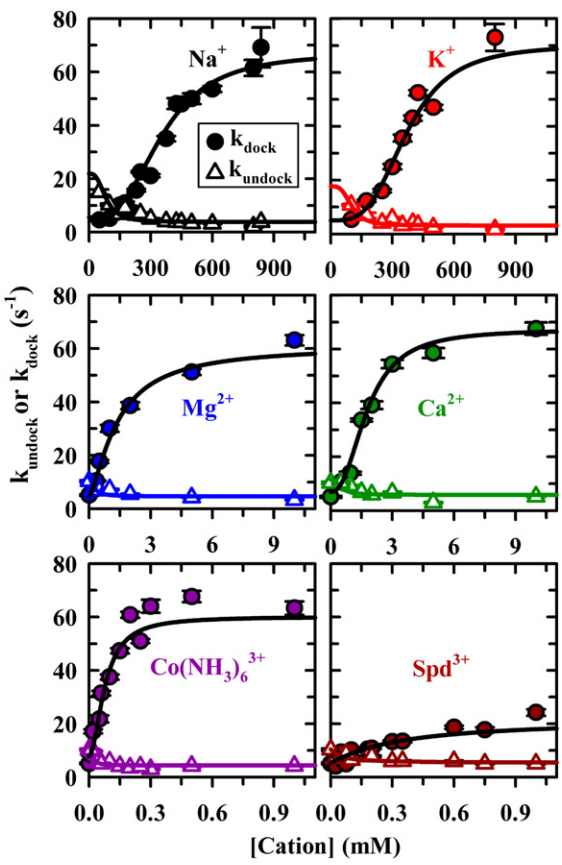

Fig. 4. [Cation] dependence of tetraloop–receptor docking/undocking kinetics. The rate constants for docking, k_{dock} (filled circles), and undocking, k_{undock} (open triangles), are plotted *versus* [cation]. Monovalents affect docking on the molar range, divalents affect docking on the 10-mM range, and trivalents affect docking on the 100- μM range. The dependence of k_{dock} and k_{undock} are fit to a four-state kinetic model (Fig. 6b), as summarized in Table 1. Note that the Spd^{3+} titration is fit to data that extend to 1.9 mM.

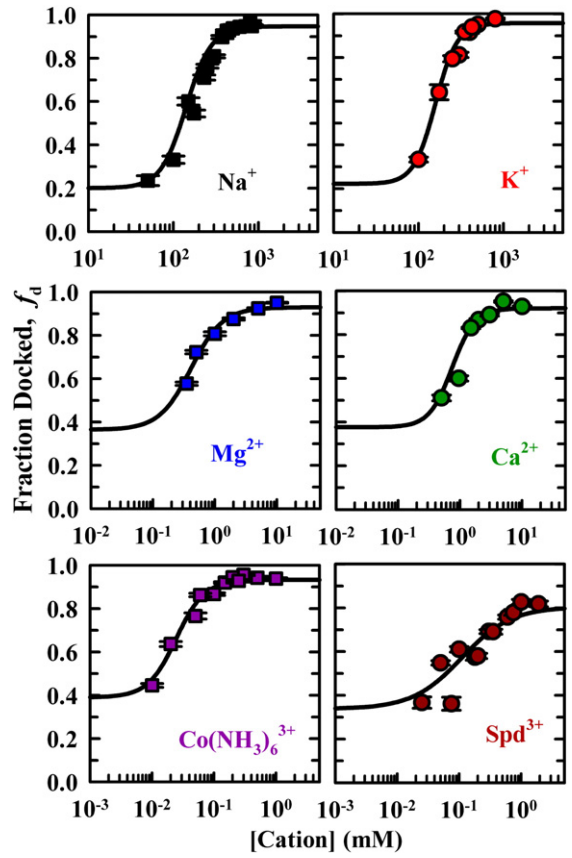

Fig. 5. Fraction of time the tetraloop–receptor construct spends in the docked state (fraction docked) as a function of cation concentration [Eq. (1)], with fits (continuous line) to the four-state kinetic model in Fig. 6b.

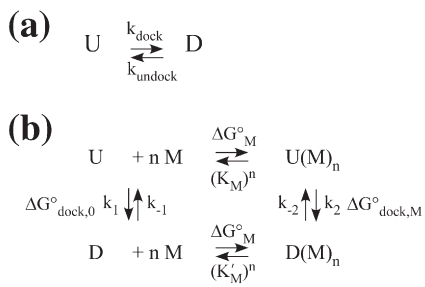

Fig. 6. Kinetic schemes for the tetraloop–receptor docking/undocking equilibrium. (a) Observed two-state kinetics for docking/undocking, where both undocked (U) and docked (D) states are affected by the ion atmosphere; thus, k_{dock} and k_{undock} are dependent on [cation]. (b) A four-state kinetic model for describing the observed [cation] dependence of k_{dock} and k_{undock}, where K_M and K'_M are the dissociation constants for the cation (M) and k_1, k_2, k_{-1}, and k_{-2} are the rate constants for docking and undocking in the cation-dependent and cation-independent pathways. The free-energy changes associated with each transition are labeled. With the use of this four-state scheme, the observed k_{dock} or k_{undock} titration is modeled as a combination of the M-dependent and M-independent pathways, the relative contributions of which are controlled by [M].

trends presented here, as will be discussed in a following section.

Once again, the clear exception in the titration trends is spermidine^{3+}, for which there is only a 4-fold increase in k_{dock} and a 1.7-fold decrease in k_{undock}. In terms of the equilibrium constant ($K_{dock} = k_{dock}/k_{undock}$), this would imply that spermidine^{3+} can only shift K_{dock} by ≈7-fold as opposed to ≈36-fold for the other cations. These cation-dependent differences in the equilibrium constant behavior are most clearly illustrated by the fraction of time the molecules spend docked, that is,

$$f_d = \frac{k_{dock}}{k_{dock} + k_{undock}} \quad (1)$$

as summarized in Fig. 5. Even under saturating [spermidine^{3+}] conditions, the RNA construct spends only ≈80% of its time docked, differing noticeably from the >95% fraction docked in the presence of all other cations investigated. There is also a steeper saturation curve for f_d compared to k_{dock} or k_{undock} alone, which requires discussion of the underlying kinetic model.

Cation-facilitated tetraloop–receptor docking: A kinetic model

Interpretation of the unusual cation concentration dependence of k_{dock} and k_{undock}, in particular, with the undocking rate constant *decreasing* with cation concentration, requires going beyond a simple two-state ion binding scheme. Such kinetics requires pathways that are dependent on and independent of the *titrated* cation, as shown in Fig. 6b. In this model first presented by Kim *et al.*, cation exchange is assumed to occur much faster than docking or undocking transitions, which is characterized by an apparent Hill coefficient, n, with dissociation constants K_M and K'_M for the undocked and docked species, respectively (Fig. 6b).[47] Furthermore, if we assume E_{FRET} for the cation-bound and cation-free forms of the docked (similarly for the undocked) states to be experimentally indistinguishable, the kinetics readily predicts single-exponential decay rates for dwell-time probabilities (Fig. 2) that depend on *both* k_1 and k_2 for docking, as well as k_{-1} and k_{-2} for undocking,[47,64] that is,

$$k_{dock} = \frac{k_1(K_M)^n + k_2[M]^n}{(K_M)^n + [M]^n} \quad (2)$$

$$k_{undock} = \frac{k_{-1}(K'_M)^n + k_{-2}[M]^n}{(K'_M)^n + [M]^n} \quad (3)$$

where M is the cation of interest. The experimental observation that k_{dock} *increases* with [M] simply requires $k_2 > k_1$, while the empirically noted *decrease* in k_{undock} with [M] mandates that $k_{-2} < k_{-1}$. Such a model has been previously applied to conformational changes in an RNA three-helix junction.[47] The thermodynamic cycle described in Fig. 6b has also been employed to theoretically link Mg^{2+} binding with RNA folding in yeast $tRNA_{Phe}$ and a ribosomal RNA fragment.[37] This scheme can be energetically described by ΔG^o_M and $\Delta G^o_{M'}$, the free energies for cation binding, and $\Delta G^o_{dock,0}$ and $\Delta G^o_{dock,M}$, the docking free energies in the absence and presence of cation, which allows for different cation affinities of the folded *versus* unfolded conformers.[24,37] The variables of the model, ΔG^o_M, $\Delta G^o_{M'}$, $\Delta G^o_{dock,0}$, and $\Delta G^o_{dock,M}$, are obtained from fitting the [cation] dependence of k_{dock} and k_{undock} (Figs. 4 and 6) and correspond to the observed [cation]-dependent docking free energy (ΔG^o_{dock}). Most importantly, since docking proceeds via some combination of the two pathways, the net uptake of cations upon docking will vary with cation concentration, as discussed later.

In the framework of this four-state kinetic model, the titrations in Fig. 4 can now be analyzed with least squares methods and explicitly compared as a function of cation charge and identity. For simplicity, the Hill coefficient in this model, n, is constrained to be common to both k_{undock} and k_{dock}. Also, k_{undock} and k_{dock} are fit simultaneously with a free-energy constraint consistent with detailed balance considerations, that is, $\Delta G^o_M + \Delta G^o_{dock,M} = \Delta G^o_{dock,0} + \Delta G^o_{M'}$, or, equivalently, $K'_M = (k_1 k_{-2}/(k_{-1} k_2))^{1/n} K_M$. The resulting weighted-least squares fits for each cation are shown along with the data in

Table 1. Cation dependence of tetraloop–receptor docking/undocking from a four-state kinetic model (Fig. 6b)

	k_1 (s^{-1})	k_{-1} (s^{-1})	k_2 (s^{-1})	k_{-2} (s^{-1})	K_M (mM)	K'_M (mM)	n
Na^{+} [a]	5±1	22±9	67±11	3.8±0.3	357±53	82±28	2.9±0.5
K^{+} [a]	5±1	18±14	70±6	3.1±0.4	371±17	102±37	3.4±0.7
Mg^{2+} [b,c]	7±2	12±3	60±11	4.5±0.5	1.5±0.7	0.24±0.18	1.7±0.5
Ca^{2+} [c]	7±2	11±3	67±12	5.8±0.5	1.8±0.4	0.53±0.24	2.4±0.7
$Co(NH_3)_6^{3+}$ [c]	8±1	12±2	60±6	4.4±0.4	0.08±0.01	0.02±0.01	1.9±0.4
Spd^{3+} [c]	5±1	10±2	22±6	5.3±0.5	0.34±0.26	0.05±0.05	1.1±0.4
Mg^{2+} (U_7) [c,d]	13±1	9±1	156±23	5.4±0.2	1.3±0.3	0.25±0.08	1.8±0.2

Parameters are determined from fits of the cation titration to a four-state model (Fig. 6b) with a detailed balance constraint of $K'_M = (k_1 k_{-2}/(k_{-1} k_2))^{1/n} K_M$.

[a] Titrations performed in 50 mM hemisodium Hepes (pH 7.5) and 100 μM EDTA. Fits of the Na^+ and K^+ titrations give independent measurements of the docking/undocking rate constants in the absence of added cation (k_1 and k_{-1}) at these buffer conditions.

[b] Data refit from Ref. 64 with the detailed balance constraint.

[c] Titrations performed in 50 mM hemisodium Hepes (pH 7.5), 100 μM EDTA, and 100 mM NaCl. Each titration fit at these conditions is an independent measurement of k_1 and k_{-1}, the docking and undocking rate constants in the absence of added cation.

[d] The A_7 linker in the RNA construct (Fig. 1a) is replaced with a U_7 linker.[65]

Fig. 4, with the fitted parameters k_1, k_{-1}, k_2, k_{-2}, K_M, K'_M, and n summarized in Table 1. The most striking observation from this table is that the individual rate constants in the model *remain identical*, within experimental error, from cation to cation! The only exception to this trend is, again, spermidine^{3+}, which we consider later. Given the enormously larger 1000-fold variations observed in the individual cation binding affinities, this is really quite a remarkable result. Indeed, these data suggest a surprising but elegantly simple interpretation—each cation, when bound in sufficient quantity to the construct, has an *equivalent ability* to promote tetraloop–receptor docking, independent of identity or charge. In the context of this model, the sensitivity to cation arises entirely from the dissociation constants themselves (K_M and K'_M), which exhibit a >1000-fold affinity range from the trivalents to monovalents. Indeed, even the modest deviations observed in k_1 (20% faster) and k_{-1} (70% slower) between multivalent and monovalent cations can be qualitatively rationalized. Specifically, the fitted k_1 and k_{-1} values represent docking/undocking rates in the *absence* of added cation concentration. However, these conditions are never sampled for the multivalent titrations due to the added 100 mM NaCl background but that, in good agreement with Table 1, would tend to further increase the docking and decrease the undocking rates.

In the context of such a kinetic model, it is the binding affinity (K_M or K'_M) that is responsible for the wide dynamic range of the [cation] docking sensitivity. Furthermore, from inspection of Table 1, it is clear that the cation *valence* rather than the cation *size* is the most important factor, at least for the isolated tetraloop–receptor tertiary interaction. Interestingly, the cation affinities are also systematically *greater* for the docked *versus* undocked conformation, that is, $K_M > K'_M$. At a more subtle level, there also appears to be an increase in the cooperativity of ion binding (n) with size of the cation, for example, Ca^{2+} appears slightly more cooperative than Mg^{2+}. Once again, the exception to this trend is spermidine^{3+}, where the three negative charges are separated by covalent bonds, and thus, size is not the only factor distinguishing it from the other cations. The substitution of the A_7 linker (Fig. 1a) with a U_7 alternative has essentially no effect on K_M, K'_M, or n (Table 1).[65] This suggests that cation uptake is intrinsic to the tetraloop–receptor docking interaction, rather than the specific linker in the construct design. By way of contrast, however, the docking rate constants (i.e., k_1 and k_2) are nearly 2-fold faster for the U_7 linker construct. This is consistent with prior expectation that the A_7 linker, which is slightly more rigid than U_7 due to base-stacking interactions, can weakly interfere with achieving the correct transition-state configuration.[65]

Discussion

The folding scheme in our isolated tetraloop–receptor construct is significantly simplified to minimize the potential for kinetic traps and folding intermediates often observed for the rugged RNA folding landscape.[45,72–74] As a result, explicit docking and undocking kinetics of a GAAA tetraloop and its receptor can offer new insight into the role of diffuse cation interactions in RNA tertiary structure formation.[62,63,66] The cations surveyed in this work all accelerate/decelerate tetraloop–receptor docking/undocking, respectively, though cation size and valence clearly play additional roles in promoting folding.

Role of valence and size in cation binding affinities

The apparent binding affinities (K_M or K'_M) for the various cations explored in this work are highly

dependent on the cation valence. For cations of the same charge, there is no discernible effect of ion size on the ion–RNA attraction strength [e.g., $K_M(Na^+) \sim K_M(K^+)$] (Table 1 and Fig. 7a and b). According to Manning condensation theory, increasing counterion charge increases a cation's ability to condense on polyanionic species such as RNA.[80] Specifically, small ions, like Mg^{2+}, can condense on the RNA at much lower concentrations than monovalents and, thereby, neutralize phosphate charges with little effect on the solution's ionic strength.[2,22,25,36,37,81] This effect is immediately evident in the data (Fig. 4) by the near-linear increase in folding rate constant with monovalent concentration *versus* a more abrupt achievement of asymptotic rate behavior for low concentrations of multivalent ions. From the counterion condensation theory of spherical polyelectrolytes, the effective residual charge per RNA phosphate after condensation (υ) can be derived as:

$$\upsilon = -(\ln\Phi)\frac{R_G}{l_b N}\frac{1}{Z} \quad (4)$$

where N is the number of nucleotides in the RNA, R_G is the radius of gyration of the polymer, l_b is the Bjerrum length (~7.1 Å in water), Z is the counterion charge, and Φ is the volume fraction of counterions ($\Phi = N_A C V_C$, where N_A is Avogadro's number, C is the concentration of the cation, and V_C is the volume per counterion).[34,80]

Thus, for the same charge neutralization (i.e., $\upsilon \approx$ constant) to be achieved, $\ln \Phi$ must scale linearly with Z. Since Φ is proportional to counterion concentration, $\ln C$ must also scale with Z to maintain the same reduction in net charge. From Eq. (4), one might expect a linear correlation of both $\ln (K_M)$ and $\ln (K_M')$ with Z because the dissociation constants correspond to the same degree of folding (Fig. 4). Indeed, a near-linear decrease of $\ln (K_M)$ and $\ln (K_M')$ with Z is observed (Fig. 7a and b). This trend implies that the free energy of ion–RNA interaction ($\Delta G^o_M/n$ and $\Delta G^o_{M'}/n$) becomes linearly more favorable with increasing Z (Table 2). A similar valence dependence of the midpoint of a folding titration in the *Tetrahymena* ribozyme was also observed.[34] Valence was also reported to be the primary determinant in the efficacy of folding stabilization in tRNA.[82] Thus, with knowledge of a single titration, one can independently estimate the dissociation constants (binding energies) for cations with the docked and undocked states as a function of valence. Though more complicated theories, such as NLPB, are needed to capture an accurate description of the ion atmosphere around the RNA,[26] counterion condensation theory offers physical insight into the observed trends.

The apparent Hill coefficient or ion binding cooperativity (n in Fig. 6b) shows sensitivity to ion size and valence, that is, it depends on charge density rather than valence alone. Specifically, n decreases with charge density, as shown in Fig. 7c. Such an observation is also anticipated from counterion condensation theory, in that fewer multivalent than monovalent cations must condense to achieve similar charge neutralization.[33,34,80,83] Furthermore, the greater the charge density, the more effectively cations screen negative charges. For example, in the absence of divalents, it would be expected that more monovalents would be required to satisfy the same charge neutralization of these regions of negative electrostatic potential. The ~1.7-fold increase in n from Mg^{2+} to Na^+ is in agreement with Poisson–Boltzmann calculations that Mg^{2+} can replace 1.9 Na^+ ions.[37] Interestingly, two distinct cation binding

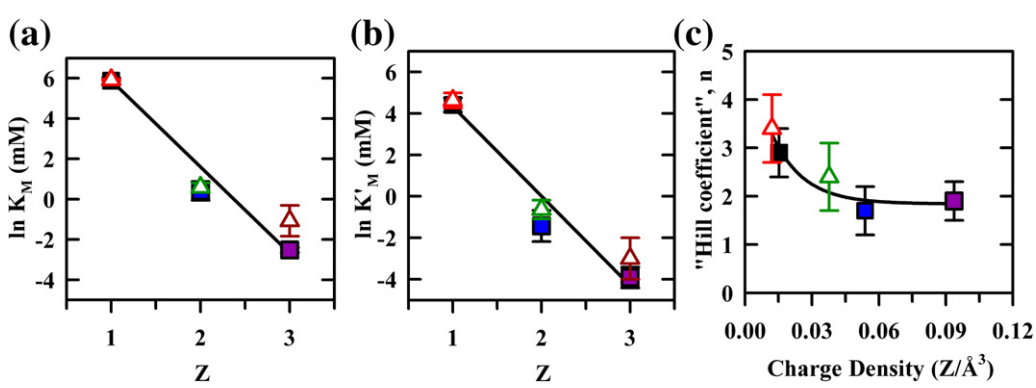

Fig. 7. Trends in apparent cation dissociation constants and Hill coefficients for cations with charge (Z) and charge density determined from the four-state kinetic model for tetraloop–receptor docking (Fig. 6b). Symbols are color coded as Na^+ (black), K^+ (red), Ca^{2+} (green), $Co(NH_3)_6^{3+}$ (purple), and spermidine^{3+} (Spd^{3+}, dark red), and the larger and smaller cations for a given charge are shown as triangles and squares, respectively. (a and b) The $\ln K_M$ and $\ln K'_M$ vary linearly with $1/Z$. (c) The Hill coefficient (n) decreases a function of charge density. Data for spermidine^{3+} are not shown because, as a polymer with distributed charges, its charge density is not a comparable parameter. An exponential fit is shown to guide the eye. For charge density determinations, see Table 2.

sites have been identified in the tetraloop–receptor interaction,[11,62] which may be reflected in a Hill coefficient of ~2 for the multivalent cations. Spermidine^{3+} is again the exception to this trend, as it exhibits the smallest n (Table 1). This effect may be due to the fact that spermidine^{3+} is simply too large a molecule to localize in small pockets of high negative charge density.

Accumulation of cations on the docked *versus* undocked RNA (ΔΓ)

Though under certain conditions, the Hill coefficient (n) may provide a good estimate for net uptake of cations with folding, ion uptake and n are in fact distinct paramaters.[69] In the kinetic model used to describe folding of the tetraloop–receptor interaction, the RNA can fold via two pathways, with both undocked and docked states accumulating cations with increasing cation concentration (Fig. 6b). The "preferential interaction coefficient" (Γ) quantifies the excess counterions around the RNA relative to the bulk solution as a function of salt concentration.[69,71,84,85] It has been shown that, under conditions where Cl^- concentration remains roughly constant with the addition of $MgCl_2$, that is, in a >30-fold excess of monovalent salt, the net Mg^{2+} uptake ($\Delta\Gamma_{2+}$) with folding can be expressed in terms of the observed [salt]-dependent standard-state free energy of docking (ΔG^o_{dock}),

$$\Delta\Gamma_{2+} = \frac{\partial ln\, K_{dock}}{\partial ln\, a_{MgCl_2}} \approx \frac{\partial ln\, K_{dock}}{\partial ln\left[Mg^{2+}\right]} = -\frac{1}{RT}\frac{\partial \Delta G^o{}_{dock}}{\partial ln\left[Mg^{2+}\right]} \quad (5)$$

where K_{dock} is the observed equilibrium constant for the docking transition and a_{MgCl2} is the molal activity of the salt.[69,85] Thus, determination of the instantaneous slope of $\Delta G^o{}_{dock}$ *versus* ln [Mg^{2+}] (Fig. 8a) is directly proportional to Mg^{2+} uptake (Fig. 8b). The plot of $\Delta G^o{}_{dock}$ *versus* ln [Mg^{2+}] is calculated from the fits of k_{dock} and k_{undock} as a function of [cation] (Fig. 4), using $K_{dock}=k_{dock}/k_{undock}$ and $\Delta G^o{}_{dock}=-RT\ln K_{dock}$. Similarly, this analysis [Eq. (5)] can be applied to all of the multivalent cations explored in this work, yielding the cation uptake of divalents and trivalents ($\Delta\Gamma_{2+}$ and $\Delta\Gamma_{3+}$; Fig. 8b).

Without an excess of Cl^-, the monovalent activity coefficient varies appreciably with salt concentration, and a slightly modified analysis is performed for assessing the monovalent ion uptake. At moderate monovalent concentrations (0–0.5 molal), the activity coefficient can be treated as a constant, and a small correction factor can be applied to the concentration-dependent salt activity when determining the slope of the $\Delta G^o{}_{dock}$ *versus* ln [M] plots to yield $2\Delta\Gamma_{\pm}$ or the ion pair uptake, representing the sum of Cl^- depletion and cation accumulation

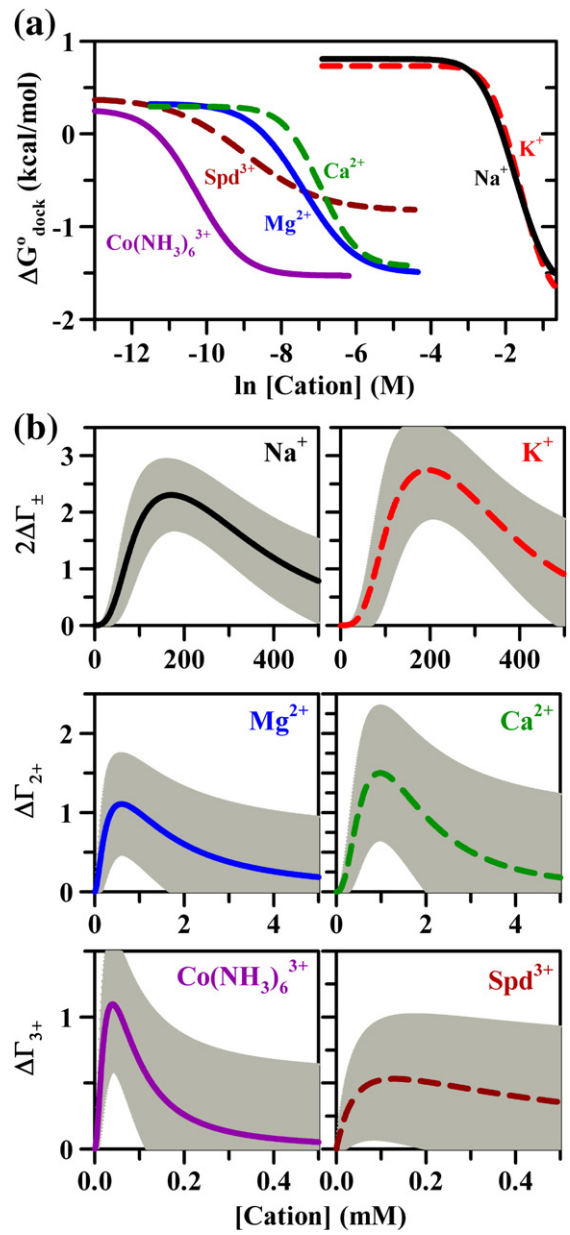

Fig. 8. Free energy for tetraloop–receptor docking and net uptake of cation with increasing [cation]. (a) A plot of $\Delta G^o{}_{dock}$ *versus* ln [cation] as calculated from the fits of k_{dock} and k_{undock} (Fig. 4) as a function of [cation], where $K_{dock}=k_{dock}/k_{undock}$ and $\Delta G^o{}_{dock}=-RT\ln K_{dock}$. (b) The net ion pair or cation uptake (ΔΓ) as a function of [cation], calculated from Eq. (5). The error bars (shown in gray) are propagated from the uncertainties in the fitted parameters (Table 1).

(Fig. 8).[71,86] Outside of this range, higher-order correction is necessary; thus, for simplicity in comparing with multivalents in Fig. 8a, we truncate the monovalent analysis to the 0- to 0.5-M range, as all trends presented in this work are still apparent. Note that this analysis assumes a constant solution

Table 2. Dependence of tetraloop–receptor docking cycle (Fig. 6b) on cations of varying charge density

	Radius (Å)	Charge density ($Z/Å^3$)	$\Delta G^o_M/n$[a]	$\Delta G^o_{M'}/n$[a]	$\Delta G^o_{dock,0}$[a]	$\Delta G^o_{dock,M}$[a]
Na^{+}[b]	2.5	0.0153	−0.60±0.08	−1.5±0.2	0.8±0.3	−1.7±0.1
K^{+}[b]	2.7	0.0121	−0.58±0.03	−1.3±0.2	0.7±0.5	−1.8±0.1
Mg^{2+}[b]	2.07	0.0538	−3.8±0.3	−4.9±0.4	0.3±0.2	−1.5±0.1
Ca^{2+}[b]	2.33	0.0377	−3.7±0.1	−4.4±0.3	0.3±0.2	−1.4±0.1
$Co(NH_3)_6^{3+}$[c]	1.97	0.0937	−5.51±0.08	−6.3±0.3	0.3±0.1	−1.5±0.1
Spd^{3+}[d]	—	0.0089	−4.7±0.4	−4.8±0.1	0.4±0.1	−0.8±0.2

$\Delta G^o_{dock,0} = -RT\ln k_1/k_{-1}$ and $\Delta G^o_{dock,M} = -RT\ln k_2/k_{-2}$.
[a] The free energy for one metal binding, $\Delta G^o_M/n = -RT\ln([M]/K_M)$ and $\Delta G^o_{M'}/n = -RT\ln([M]/K'_M)$, where [M] = 1 M at standard-state conditions and T is room temperature (294 K).
[b] Radius is defined as the metal–oxygen distance for hydrated cations.[75–77]
[c] Radius is defined as the Co–N bond length.[78]
[d] Density calculated using van der Waals volume of 337 Å^3.[79]

density with added monovalent salt; indeed, the density only varies ~1% over the concentration range explored, which is less than the measurement uncertainty.[71]

At low [cation] concentrations, the uptake is ~0, followed by a steep rise that reaches a maximum at a value near the Hill coefficient (Fig. 8b). At high [cation], the uptake decreases with concentrations, since the addition of salt minimally affects the docking equilibrium constant as the ion atmosphere of the undocked RNA saturates. As expected from the Hill coefficients (Fig. 7c), the uptake correlates with charge density. Measurements of $\Delta\Gamma$ for a series of group I monovalent cations (e.g., Na^+ and K^+) for the bimolecular dual tetraloop–receptor complex also support that charge density (or ion size) alters ion uptake.[86] Similarly, valence and size effects are also noted in single-molecule measurements of tRNA folding.[82] Our observation that the net cation uptake is dependent on concentration is consistent with explicit measurements of excess Mg^{2+} on unfolded and folded RNAs.[69] To facilitate comparison with literature, we determine the peak value of ion uptake plots (Fig. 8b), as this parameter appropriately describes the commonly reported concentration region over which the ΔG^o_{dock} *versus* ln [M] curve decreases with a maximum, constant slope (Fig. 8a and Table 3). Indeed, these results compare remarkably well with the ≈2-fold higher Mg^{2+}, K^+, and Na^+ values observed in bimolecular studies of a dual tetraloop–receptor construct, as would be expected for simple superposition of two identical tertiary interactions.[66,86]

In summary, analysis of the tetraloop–receptor docking process in terms of the four-state kinetic model, facilitated by knowledge of both k_{dock} and k_{undock}, reveals a critical feature of RNA–ion interactions; specifically, cation uptake can vary as a function of ion concentration and charge density, even for cations of the same valence (Fig. 8b).[69,86] This observation supports that RNA–ion interaction theories must incorporate size effects to explain the curvature of a cation titration.[26,32] Furthermore, these results emphasize that cation uptake with folding can be significant, and therefore, both unfolded and folded states must be considered to correctly predict the thermodynamics of folding as a function of salt concentration.

Effect of cations on the docking reaction coordinate

As illustrated in Fig. 4, the behavior of k_{dock} and k_{undock} is well characterized by a kinetic model with cation-dependent and cation-independent contributions (Fig. 6b). It is important to stress that this model neither implies nor requires dual transition states for every docking "reaction" but, rather, a single transition state for the observed two-state docking process that is itself a function of cation concentration (Fig. 6a). The detailed impact of cation-induced changes in this single transition state can be well represented by a kinetic model with two extreme rate pathways (k_1 without cations and k_2 under saturating cation conditions), though clearly all folding events take place at one intermediate cation concentration. The net effect is docking described by an effective unimolecular rate constant, expressed in Eqs. (2) and (3) in terms of ion concentration ([M]), ion dissociation constants (K_M and K'_M), k_1, and k_2.[47,64,65] Such a four-state model is particularly informative in that it allows quantitative extraction of preferential cation interactions with the transition state and the docked state *versus* the undocked state. The previous section (Fig. 8b) demonstrated a net accumulation of cations in the docking process, indicating that the docked

Table 3. Maximum ion uptake ($\Delta\Gamma^{\ddagger}$ and $\Delta\Gamma$) and counterion stabilization of the docked state and transition state with respect to the undocked state

	$\Delta\Gamma^{\ddagger}$	$\Delta\Gamma$	$\Delta\Delta G^{\ddagger}_{dock}$	$\Delta\Delta G^o_{dock}$
Na^+	1.6±0.5	2.3±0.6	−1.5±0.2	−2.5±0.3
K^+	2.2±0.3	2.7±0.9	−1.5±0.2	−2.6±0.5
Mg^{2+}	0.8±0.6	1.1±0.6	−1.3±0.2	−1.8±0.2
Ca^{2+}	1.2±0.5	1.5±0.8	−1.3±0.2	−1.7±0.2
$Co(NH_3)_6^{3+}$	0.9±0.1	1.1±0.5	−1.2±0.1	−1.8±0.1
Spd^{3+}	0.4±0.4	0.53±0.48	−0.8±0.2	−1.2±0.2

state has a higher affinity for cations than the undocked state, attributable to an increase in negative charge density. This fact is also simply revealed from the kinetic model analysis in the observation that $K_M > K_M'$. This analysis [Eq. (5)] can also be used to characterize the transition state (via k_{dock}) by quantifying again the ion uptake parameter $\Delta\Gamma^{\ddagger}$ from $\partial \ln k_{dock}/\partial \ln a_{salt}$, where a_{salt} is the activity of the salt.

To illustrate features common to all of the cations, we show an example of the resulting Mg^{2+} uptake ($\Delta\Gamma^{\ddagger}{}_{2+}$) for the transition state *versus* $\Delta\Gamma_{2+}$ of the docked state (Fig. 9a). The cation uptake is steeper and rises to a larger value for the overall docking process than for formation of the transition state.

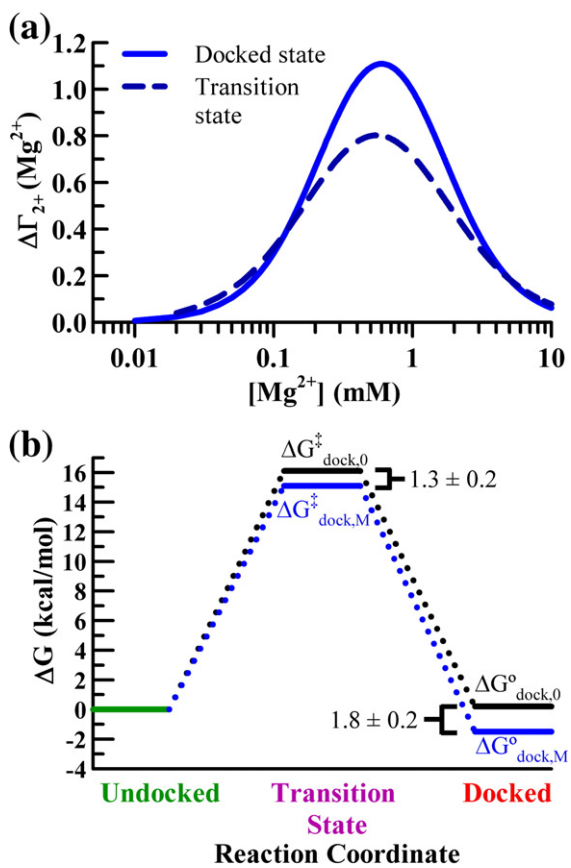

Fig. 9. Cation dependence of the tetraloop–receptor docking reaction. (a) Cation uptake for the transition state ($\Delta\Gamma^{\ddagger} = \partial \ln k_{dock}/\ln[Mg^{2+}]$) and docked state ($\partial \ln k_{dock}/\ln[Mg^{2+}]$), plotted as a function of $[Mg^{2+}]$. The curves are calculated from the fits of k_{dock} and K_{dock} *versus* $[Mg^{2+}]$. (b) Change in free energy (kcal/mol) for tetraloop–receptor docking/undocking in the absence of and at saturating $[Mg^{2+}]$ in a background of 100 mM NaCl. The barrier and overall free-energy changes in the presence and absence of Mg^{2+} are estimated from the fit parameters (Table 1), as $\Delta G^{o}_{dock,0} = -RT\ln(k_1/k_{-1})$, $\Delta G^{o}_{dock,M} = -RT\ln(k_2/k_{-2})$, $\Delta G^{\ddagger}_{dock,0} = -RT\ln(k_1/\nu)$, and $\Delta G^{\ddagger}_{dock,M} = -RT\ln(k_2/\nu)$ with an estimate of $\nu \approx 10^{13}$.

This observation implies that though both the docked state and the transition state are stabilized by counterions, the docked state has a steeper salt dependence than the transition state and thus must be preferentially stabilized. The transition state systematically acquires 70–80% of the ion uptake required by the docked state (Fig. 9a, Fig. S3, and Table 3), suggesting similar transition-state structures in the presence of each cation. The large accumulation of cations in the transition state supports the notion that the transition state is compact and, therefore, requires uptake of counterions to screen helical repulsions.[35,65–67] We have previously suggested that the transition state for docking is early, that is, lacking the hydrogen-bonded tertiary interaction (Fig. 1b).[65] The marked additional uptake of ions from the transition state to the docked state may also suggest other unique structural differences between the transition state and the docked state, such as additional compaction or receptor rearrangement. Based on linker control of accessible volume and therefore relative concentration of tetraloop and receptor, our measurements of the *unimolecular* docking rate constant and cation uptake are also in excellent agreement with *bimolecular* association values measured for Mg^{2+} and K^{+} for a dual tetraloop–receptor construct (J. L. Fiore and D. J. Nesbitt, unpublished results).[66]

The net result of the higher affinity for cations in the docked and transition state *versus* the undocked state is that both the barrier height for docking and the overall all free energy for docking decrease with counterion concentration. In other words, k_{dock} increases with [cation], but since the reverse barrier height for undocking increases, there is also a corresponding decrease in k_{undock}, as shown in Fig. 4. To illustrate this point in terms of a reaction coordinate, we calculate the overall ΔG^{o}_{dock} for docking under saturating $[Mg^{2+}]$ and in the absence of Mg^{2+} (Fig. 9b). In an analogous fashion, the barrier height for docking $\Delta G^{\ddagger}_{dock}$ can be estimated from generalized transition-state theory, k_{dock} as:

$$k_{dock} = \nu e^{\left(-\Delta G^{\ddagger}_{dock}/RT\right)} \tag{6}$$

where $\Delta G^{\ddagger}_{dock}$ is the activation free energy and ν is the attempt frequency for barrier crossing.[65,67,87,88] Absolute determination of $\Delta G^{\ddagger}_{dock}$ requires knowledge of ν; an estimate of $\nu \approx 10^{13}\ s^{-1}$ is sufficient for our current purposes, since the dependence of the reaction rate on this parameter is only logarithmic.[65,67,89,90] It is important to emphasize, however, that all reported experimental changes in the barrier height (i.e., $\Delta\Delta G^{\ddagger}_{dock}$) are rigorously independent of this choice of ν [Eq. (6)]. The net effect of Mg^{2+} on the free-energy reaction coordinate is shown in Fig. 9b.

The effects of each cation on the reaction coordinate are summarized in Table 3. Rather remarkably,

the same maximum docking frequency (Fig. 4) is quite similar for all cations investigated, with the exception of spermidine^{3+}, which we discuss at the end of this section. Thus, the ~12-fold increase in docking rate with increasing concentration of these cations (Fig. 4) translates into a universal ~1 kcal/mol decrease in the activation barrier, whereas the docked state appears to be stabilized by about twice that amount (Table 3). Free-energy folding barriers on the order of the ≈15 kcal/mol values observed herein are common for RNA tertiary folding. For example, the barrier height for folding of the P4–P6 domain is ≈16 kcal/mol at 35 °C at 10 mM Mg^{2+}.[91]

The only exception to this trend is spermidine^{3+}, which, despite K_M values comparable with $Co(NH_3)_6^{3+}$, exhibits a diminished effect on k_{dock} and k_{undock}. Specifically, there is now only an ~4-fold *versus* ~12-fold increase in docking rate and, therefore, a notably smaller *decrease* in the overall favorability (i.e., $\Delta\Delta G^{o}_{dock}$) for the docking event (Table 3). The origin of this decreased ability of spermidine^{3+} to enable docking can be rationalized in terms of its structure. In contrast with atomic cations, spermidine^{3+} is a large flexible molecule with charges distributed along a chain (Fig. 2). Therefore, when such polyatomic counterions condense on the RNA, steric hindrance may prevent proper localization in regions of high negative charge density, preventing full screening of electrostatic repulsions. With its large size, repulsions between spermidine^{3+} ions can also become important and prevent further condensation of additional cations. In such a kinetic picture, the RNA molecule may still be "saturated" with spermidine^{3+} yet fully screened. As a result, k_{dock} and k_{undock} can saturate with a lower dynamic range than for the smaller cations. This effect is not unprecedented; for example, spermidine^{3+} was shown to stabilize the folded *Tetrahymena* ribozyme less effectively and induce less compact structures than $Co(NH_3)_6^{3+}$.[33,34] Additionally, in studying the role of polyamines on the folding of the *Tetrahymena* ribozyme, it was observed that when excluded volumes become significant, folding does not go to completion,[79] similar to what is seen here for tetraloop–receptor folding. In related ensemble investigations of the *Tetrahymena* ribozyme, it was also shown that the transition states[75] become broader and less compact as the polyamine cation chain becomes increasingly larger. We thus postulate similar dynamics as the origin of the reduced effects of spermidine^{3+} on lowering barrier heights for the isolated tetraloop–receptor tertiary interaction when compared to the atomic cations.

Mechanisms of cation-facilitated tetraloop–receptor docking

We have recently shown that both [Mg^{2+}]- and [monovalent]-facilitated tetraloop–receptor docking are primarily entropic in origin.[65,67] However, though the overall thermodynamic stabilization is similar for Mg^{2+} *versus* monovalent cations (Fig. 4), the underlying entropic and enthalpic contributions are strikingly different.[65–67] Specifically, we showed that monovalent cations such as Na^+ and K^+ decrease the overall entropic cost of docking much more significantly than Mg^{2+}.[65,67] We can now offer the cation uptake curves in Fig. 8 to provide insight into entropic mechanisms of [cation]-facilitated docking. One putative mechanism would be a reduction in the entropic penalty of counterion uptake,[83,84] which is required to combat electrostatic repulsion as the RNA folds and creates pockets of negative electrostatic potential.[65]

Such an entropic benefit can be rationalized from analysis of the net cation uptake curves in Figs. 8 and 9a (and Fig. S3). Consider, for example, the multivalent titrations, which begin at 100 mM NaCl (Fig. 8b). Mg^{2+} uptake is constant over the steepest part of the [Mg^{2+}]-dependent docking curve in Fig. 8; thus, addition of Mg^{2+} to the bulk solution lowers the entropic cost of Mg^{2+} uptake, as previously described using thermodynamic data and arguments.[65] Similarly, Mg^{2+} may reduce the number of Na^+ ions required to fold, since RNA has the option to preferentially take up the more strongly interacting divalent ions. Mg^{2+} can also satisfy the necessary screening with fewer ions than Na^+, as seen by the maximum uptake, where the net accumulation of Mg^{2+} is ~1.1 Mg^{2+} ions *versus* ~2.3 Na^+ ions (Table 3). Therefore, increasing multivalent [cation] may aid folding both by decreasing the entropic cost of localizing cations and/or by decreasing the number of cations needed to fold.[65]

In the case of monovalent species, however, more cations are taken up as concentration is increased, an effect that reduces any net entropic benefit to counterion reorganization. Thus, other factors may play a more significant role in promoting docking, as discussed elsewhere.[67] For example, increasing monovalent [cation] can change the unfolded structures of the RNA, for example, by organizing the receptor structure or increasing base stacking in the poly(A) linker, which can alter RNA folding thermodynamics by reducing the conformational entropy of the undocked state.[65–67,92,93] Effects of hydration may also play a role.[66] Thus, though the net saturation effect of adding monovalent and multivalent cations on the overall single-molecule docking kinetics is strikingly similar, clearly, one must take into account more subtle aspects of the ion–RNA interactions to appropriately deconstruct the underlying thermodynamic contributions.

Due to the hierarchical nature of RNA folding, flexible junctions can enable unpaired nucleotides to act as beacons between helical regions.[17,50,51] In this

regard, the building blocks of RNA structural assembly are helix–junction–helix motifs, with folding mediated by tertiary interactions.[39,94] The tetraloop–receptor tertiary interaction is exceptionally common[54–57] and even more generally categorized as the A-minor motif—adenosine insertion into a distal minor groove.[11,52,95,96] However, it is also relevant to note that the A_7 linker (Fig. 1) used in this construct may contribute to the folding thermodynamics and kinetics.[63,65] Junctions such as the A_7 linker limit the conformations of unfolded states[94,97,98] and can be affected by cation-induced stiffening.[65,92,93] One particularly important observation is that the tetraloop–receptor interaction apparently dictates the ion–RNA interactions of docking, as shown by the indistinguishable K_M and K'_M values for Mg^{2+} in the A_7 *versus* U_7 linked constructs (Table 1). In further support of this notion is the remarkable similarity between the cation uptake (Table 3) reported in this work and that observed in the bimolecular association of modular tetraloop–receptor constructs, as mentioned above.[66] Therefore, a clear conclusion would be that studies of the tetraloop–receptor construct report on trends of cation-mediated helical packing more generally applicable to other tertiary interactions.

Summary and Conclusion

A two-state ion binding scheme is insufficient to explain the origin of [cation]-dependent k_{dock} and k_{undock} rate constants for the tetraloop–receptor interaction. However, a four-state kinetic model is able to accurately recapitulate the experimentally observed increase in k_{dock} and decrease in k_{undock} with [cation], whereby the cations are more attracted to the docked than undocked RNA. With this model, we can separate the free energies of cation–RNA interactions from the kinetics of docking/undocking. Furthermore, this model allows for quantitation of the differential affinities for cations in the folded and unfolded conformations of the RNA. In addition, we have determined the effective cation uptake with folding by way of the preferential interaction coefficient. The results indicate that both ion charge density and valence affect the preferential cationic interaction with the docked *versus* undocked RNA, which should provide useful benchmark data for testing theoretical models for ion–RNA interactions.[1] However, cation valence plays the major role in determining the cation concentration range required for promotion of folding. Quite remarkably, monovalent, divalent, and trivalent cations under saturating conditions achieve the same asymptotic folding rate. The notable exception to this trend is polycationic spermidine^{3+}, which is 3-fold less effective at promoting docking than trivalent $Co(NH_3)^{3+}$ and for which the extended size likely prevents the localization of charge needed to properly screen negative charge and thereby fully enhance the folding rate. Finally, utilization of a four-state kinetic model reveals a possible physical origin of the cation dependence in terms of the decreased entropic penalty of cation uptake with folding.

Materials and Methods

RNA preparation

Cy3-labeled and Cy5-labeled tetraloop–receptor constructs (Fig. 1a) are prepared as previously described.[63,64] Briefly, synthetic 5′ three carbon amino-modified RNA oligomers (Dharmacon, Lafayette, CO)† are labeled with Cy3 and Cy5 *N*-succinimidyl esters (Amersham Biosciences, Piscataway, NJ) and HPLC purified. We anneal the Cy3 (1 μM) and Cy5 (1.5 μM) RNA oligomers with 2 μM biotinylated DNA oligomer (Integrated DNA Technologies, Coralville, IA) by heating to 70 °C and cooling slowly to room temperature in a buffer of 50 mM hemisodium Hepes, 100 mM NaCl, and 100 μM ethylenediaminetetraacetic acid (EDTA) at pH 7.5, which forms the complete construct (Fig. 1a). The secondary structure of the Cy3 strand forms the tetraloop with an A_7 linker connecting it to the receptor domain created by the hybridized Cy3 and Cy5 strands. Molecules are tethered to streptavidin-coated glass surfaces with the biotinylated extension formed by the hybridized DNA and Cy5 strands.

Single-molecule FRET measurements

To enable single-molecule FRET studies of immobilized RNA, we have exploited a scanning confocal microscope system, as previously described.[36,64] Excitation of the donor Cy3 chromophore is obtained via a 532-nm mode-locked pulsed-laser operating at 82 MHz (Model 3800; Spectra Physics), with donor and acceptor emission discriminated by dichroic beamsplitters and bandpass filters and detected on single-photon counting avalanche photodiodes (SPCM-AQR-14; Perkin-Elmer Optoelectronics, Fremont, CA).[64] Fluorescence trajectories are acquired for individual RNA constructs located on the cover glass by an intensity search algorithm, with time traces acquired using a time-correlated single-photon counting module (SPC-134; Becker & Hickl, Berlin).

RNA constructs are immobilized on a cover glass in a microfluidic flow-cell assembly[36,64] and observed in the diffraction-limited laser focus (objective numerical aperture, 1.2) at 1- to 1.7-μW laser powers measured at the back plane of the microscope. A protocatechuic acid/protocatechuate-3,4-dioxygenase enzymatic oxygen scavenging solution

† Mention of commercial products is for information only; it does not imply National Institute of Standards and Technology recommendation or endorsement nor does it imply that products mentioned are necessarily the best available for the purpose.

(5 mM protocatechuic acid and 60 nM protocatechuate-3,4-dioxygenase) with 2 mM Trolox is added for fluorophore photostability.[99,100] Divalent (Mg^{2+} and Ca^{2+}) and trivalent [$Co(NH_3)^{3+}$ and spermidine^{3+}] titrations are performed in a standard buffer containing 50 mM hemisodium Hepes (pH 7.5 at 25 °C), 100 mM NaCl, and 0.1 mM EDTA, with varying concentrations of $MgCl_2$, $CaCl_2$, hexamine cobalt trichloride, and spermidine trihydrochloride. Freshly prepared spermidine stock solutions are aliquoted and kept frozen to avoid deamination, as suggested by the manufacturer. At pH 7.5, spermidine has a nominally +3 charge ($pK_{a1}=8.6$, $pK_{a2}=10.0$, and $pK_{a3}=11.1$; thus, 93% of the time the amino groups are deprotonated).[101] Monovalent (K^+ and Na^+) studies of the tetraloop–receptor motif are performed in 50 mM hemisodium Hepes (pH 7.5) and 0.1 mM EDTA, with [NaCl] and [KCl] varied. We note, however, that this buffer already contains 25 mM Na^+ in the absence of any added NaCl; therefore, the reported cation concentrations refer to *added* amounts of the respective salt. All buffers are 0.2 μm sterile filtered and prepared using liquid chromatography–mass spectrometry Chromosolv H_2O. After flushing in solutions, data are collected under static conditions, with entrance and exit holes covered by tape. All experiments are performed at 21 °C.

Single-molecule trajectory analysis

The FRET efficiency, E_{FRET}, is calculated ratiometrically from the donor and acceptor signals for time trajectories binned at 5–10 ms, which clearly resolves the undocked and docked states.[36,64] The corrected intensity-based FRET efficiency (E_{FRET}) is calculated from the background subtracted signals on the two channels, ΔI_1 and ΔI_2, designed primarily for donor and acceptor detection, respectively. Corrections are implemented for (i) collection efficiencies and cross talk of the donor and acceptor emission on channels 1 and 2 (β_1^A, β_2^A, β_1^D, β_2^D), (ii) differential quantum yields of the donor and acceptor (Q_D and Q_A), and (iii) direct laser excitation of the donor and acceptor (α_D,α_A, where $\alpha_D+\alpha_A=1$),

$$E_{FRET} = \frac{\beta_1^D \Delta I_2 - \beta_2^D \Delta I_1 - \frac{\alpha_A}{\alpha_D}\frac{Q_A}{Q_D}\left(\beta_2^A \Delta I_1 - \beta_1^A \Delta I_2\right)}{\beta_1^D \Delta I_2 - \beta_2^D \Delta I_1 + \frac{Q_A}{Q_D}\left(\beta_2^A \Delta I_1 - \beta_1^A \Delta I_2\right)} \quad (7)$$

where the relevant quantum yield ratios and collection efficiencies are determined from independent measurements.[36] Relative direct laser excitation of the acceptor *versus* donor is calculated from extinction coefficients at 532 nm.[36] Donor-only species, clearly identifiable by the absence of acceptor emission, are observed with a low frequency (<15%) and can be disregarded. Day-to-day reproducibility of the center E_{FRET} values is ±0.02. The quantum yield ratio (Q_A/Q_D) is independent of the cation concentration, as assessed by fluorescence lifetime measurements of singly labeled constructs (see Supplementary Information: Supplementary Text and Fig. S1). Cy3 and Cy5 are weakly quenched by cobalt hexamine. However, the degree of quenching for both fluorophores is equal within uncertainty, such that the quantum yield ratio in Eq. (7) is maintained. Furthermore, the Förster radius (R_0) remains constant (see Supplementary Information and Fig. S1).[102] Thus, the low and high E_{FRET} states correspond to the undocked and docked RNAs at varying cation concentrations.

Docking and undocking rate constants from single-molecule trajectories

To determine docking and undocking rate constants at each cation concentration, we define dwell times of the tetraloop–receptor construct in the docked and undocked conformations by the crossing of a threshold set at the minimum of the bimodal E_{FRET} distribution in the real-time trajectory. As shown elsewhere, histograms of the dwell times in the docked and undocked states at a given cation concentration can be converted into probability densities, $P(\tau_i)=H(\tau_i)/[0.5(\tau_{i+1}-\tau_{i-1})]$, where $H(\tau_i)$ is the standard histogram value and τ_i represents an ordered list of nonzero time bins, significantly enhancing the dynamic range of observable timescales.[64,103] The resulting dwell-time histograms and normalized probability densities [$P(\tau)/P(0)$] are well described by single-exponential decays for both docking and undocking events, with least squares single-exponential fits yielding rate constants, k_{dock} and k_{undock}. Data sets contain a minimum of 200 (but more typically 500) events. By way of validation, hidden Markov modeling is also pursued as an alternative method for determining rate constants; the results yield identical rate constants within experimental uncertainties, as expected for a system with two well-resolved fluorescent states.[104]

Tetraloop–receptor folding is known to be kinetically heterogeneous, yielding three subset populations: (i) a majority population (68%) that actively switches between the docked and undocked conformations, (ii) a minority population (32%) that does not dock on the timescale of observation, and (iii) an extremely small population (~1%) of molecules remaining in a high E_{FRET} state.[64] As discussed elsewhere, the origin of this heterogeneity is not well understood[36,105] but is observed to remain at a constant 32% fraction over the 4 orders of magnitude range of cationic environments explored here. Since the two minority populations provide no docking/undocking information on the timescale of the experiment, they can be cleanly separated and excluded from the analysis.

Acknowledgements

This work was supported in part by the National Science Foundation, National Institute of Standards and Technology, and W. M. Keck Foundation initiative in RNA sciences at the University of Colorado at Boulder. J.L.F. was supported in part by the Optical Science and Engineering Program of National Science Foundation Integrative Graduate Education and Research Traineeship. J.L.F. and E.D.H. were supported in part by National Institutes of Health/University of Colorado Biophysics Training (T32 GM-065103) grant. We acknowledge Drs. Arthur Pardi and Christopher D. Downey for the design and preparation of the RNA constructs used in this work.

Supplementary Data

Supplementary data to this article can be found online at http://dx.doi.org/10.1016/j.jmb.2012.07.006

References

1. Draper, D. E. (2004). A guide to ions and RNA structure. *RNA*, **10**, 335–343.
2. Woodson, S. A. (2005). Metal ions and RNA folding: a highly charged topic with a dynamic future. *Curr. Opin. Chem. Biol.* **9**, 104–109.
3. Froschauer, E. M., Kolisek, M., Dieterich, F., Schweigel, M. & Schweyen, R. J. (2004). Fluorescence measurements of free [Mg^{2+}] by use of mag-fura 2 in *Salmonella enterica*. *FEMS Microbiol. Lett.* **237**, 49–55.
4. Cayley, S., Lewis, B. A., Guttman, H. J. & Record, M. T. (1991). Characterization of the cytoplasm of *Escherichia coli* K-12 as a function of external osmolarity: implications for protein–DNA interactions *in vivo*. *J. Mol. Biol.* **222**, 281–300.
5. London, R. E. (1991). Methods for measurement of intracellular magnesium: NMR and fluorescence. *Annu. Rev. Physiol.* **53**, 241–258.
6. Igarashi, K. & Kashiwagi, K. (2000). Polyamines: mysterious modulators of cellular functions. *Biochem. Biophys. Res. Commun.* **271**, 559–564.
7. Tabor, C. W. & Tabor, H. (1984). Polyamines. *Annu. Rev. Biochem.* **53**, 749–790.
8. Draper, D. E. (2008). RNA folding: thermodynamic and molecular descriptions of the roles of ions. *Biophys. J.* **95**, 5489–5495.
9. Anderson, C. F. & Record, M. T. (1995). Salt–nucleic acid interactions. *Annu. Rev. Phys. Chem.* **46**, 657–700.
10. Cate, J. H. & Doudna, J. A. (1996). Metal-binding sites in the major groove of a large ribozyme domain. *Structure*, **4**, 1221–1229.
11. Cate, J. H., Gooding, A. R., Podell, E., Zhou, K. H., Golden, B. L., Kundrot, C. E. *et al.* (1996). Crystal structure of a group I ribozyme domain: principles of RNA packing. *Science*, **273**, 1678–1685.
12. Correll, C. C., Freeborn, B., Moore, P. B. & Steitz, T. A. (1997). Metals, motifs, and recognition in the crystal structure of a 5S rRNA domain. *Cell*, **91**, 705–712.
13. Pley, H. W., Flaherty, K. M. & McKay, D. B. (1994). Three-dimensional structure of a hammerhead ribozyme. *Nature*, **372**, 68–74.
14. Draper, D. E., Grilley, D. & Soto, A. M. (2005). Ions and RNA folding. *Annu. Rev. Biophys. Biomol. Struct.* **34**, 221–243.
15. Draper, D. E. & Misra, V. K. (1998). RNA shows its metal. *Nat. Struct. Biol.* **5**, 927–930.
16. Misra, V. K. & Draper, D. E. (1998). On the role of magnesium ions in RNA stability. *Biopolymers*, **48**, 113–135.
17. Tinoco, I. & Bustamante, C. (1999). How RNA folds. *J. Mol. Biol.* **293**, 271–281.
18. Bloomfield, V. A., Wilson, R. W. & Rau, D. C. (1980). Polyelectrolyte effects in DNA condensation by polyamines. *Biophys. Chem.* **11**, 339–343.
19. Bloomfield, V. A. (1991). Condensation of DNA by multivalent cations: considerations on mechanism. *Biopolymers*, **31**, 1471–1481.
20. Braunlin, W. H., Strick, T. J. & Record, M. T., Jr (1982). Equilibrium dialysis studies of polyamine binding to DNA. *Biopolymers*, **21**, 1301–1314.
21. Wemmer, D. E., Srivenugopal, K. S., Reid, B. R. & Morris, D. R. (1985). Nuclear magnetic resonance studies of polyamine binding to a defined DNA sequence. *J. Mol. Biol.* **185**, 457–459.
22. Bai, Y., Greenfeld, M., Travers, K. J., Chu, V. B., Lipfert, J., Doniach, S. & Herschlag, D. (2007). Quantitative and comprehensive decomposition of the ion atmosphere around nucleic acids. *J. Am. Chem. Soc.* **129**, 14981–14988.
23. Sharp, K. A., Friedman, R. A., Misra, V., Hecht, J. & Honig, B. (1995). Salt effects on polyelectrolyte–ligand binding: comparison of Poisson–Boltzmann, and limiting/law counterion binding models. *Biopolymers*, **36**, 245–262.
24. Misra, V. K., Shiman, R. & Draper, D. E. (2003). A thermodynamic framework for the magnesium-dependent folding of RNA. *Biopolymers*, **69**, 118–136.
25. Chin, K., Sharp, K. A., Honig, B. & Pyle, A. M. (1999). Calculating the electrostatic properties of RNA provides new insights into molecular interactions and function. *Nat. Struct. Biol.* **6**, 1055–1061.
26. Chu, V. B., Bai, Y., Lipfert, J., Herschlag, D. & Doniach, S. (2008). A repulsive field: advances in the electrostatics of the ion atmosphere. *Curr. Opin. Chem. Biol.* **12**, 619–625.
27. Anthony, P. C., Sim, A. Y. L., Chu, V. B., Doniach, S., Block, S. M. & Herschlag, D. (2012). Electrostatics of nucleic acid folding under conformational constraint. *J. Am. Chem. Soc.* **134**, 4607–4614.
28. Tan, Z.-J. & Chen, S.-J. (2011). Salt contribution to RNA tertiary structure folding stability. *Biophys. J.* **101**, 176.
29. Tan, Z. J. & Chen, S. J. (2011). Importance of diffuse metal ion binding to RNA. *Met. Ions Life Sci.* **9**, 101–124.
30. Koculi, E., Hyeon, C., Thirumalai, D. & Woodson, S. A. (2007). Charge density of divalent metal cations determines RNA stability. *J. Am. Chem. Soc.* **129**, 2676–2682.
31. Chu, V. B. & Herschlag, D. (2008). Unwinding RNA's secrets: advances in the biology, physics, and modeling of complex RNAs. *Curr. Opin. Struct. Biol.* **18**, 305–314.
32. Chu, V. B., Bai, Y., Lipfert, J., Herschlag, D. & Doniach, S. (2007). Evaluation of ion binding to DNA duplexes using a size-modified Poisson–Boltzmann theory. *Biophys. J.* **93**, 3202–3209.
33. Heilman-Miller, S. L., Pan, J., Thirumalai, D. & Woodson, S. A. (2001). Role of counterion condensation in folding of the *Tetrahymena* ribozyme II. Counterion-dependence of folding kinetics. *J. Mol. Biol.* **309**, 57–68.
34. Heilman-Miller, S. L., Thirumalai, D. & Woodson, S. A. (2001). Role of counterion condensation in folding of the *Tetrahymena* ribozyme. I. Equilibrium stabilization by cations. *J. Mol. Biol.* **306**, 1157–1166.
35. Bokinsky, G., Rueda, D., Misra, V. K., Rhodes, M. M., Gordus, A., Babcock, H. P. *et al.* (2003). Single-

molecule transition-state analysis of RNA folding. *Proc. Natl Acad. Sci. USA*, **100**, 9302–9307.
36. Fiore, J. L., Hodak, J. H., Piestert, O., Downey, C. D. & Nesbitt, D. J. (2008). Monovalent and divalent promoted GAAA tetraloop–receptor tertiary interactions from freely diffusing single-molecule studies. *Biophys. J.* **95**, 3892–3905.
37. Misra, V. K. & Draper, D. E. (2002). The linkage between magnesium binding and RNA folding. *J. Mol. Biol.* **317**, 507–521.
38. Soto, A. M., Misra, V. & Draper, D. E. (2007). Tertiary structure of an RNA pseudoknot is stabilized by "diffuse" Mg^{2+} ions. *Biochemistry*, **46**, 2973–2983.
39. Bai, Y., Chu, V. B., Lipfert, J., Pande, V. S., Herschlag, D. & Doniach, S. (2008). Critical assessment of nucleic acid electrostatics via experimental and computational investigation of an unfolded state ensemble. *J. Am. Chem. Soc.* **130**, 12334–12341.
40. Zhuang, X. W., Kim, H., Pereira, M. J. B., Babcock, H. P., Walter, N. G. & Chu, S. (2002). Correlating structural dynamics and function in single ribozyme molecules. *Science*, **296**, 1473–1476.
41. Tan, E., Wilson, T. J., Nahas, M. K., Clegg, R. M., Lilley, D. M. J. & Ha, T. (2003). A four-way junction accelerates hairpin ribozyme folding via a discrete intermediate. *Proc. Natl Acad. Sci. USA*, **100**, 9308–9313.
42. Smith, G. J., Lee, K. T., Qu, X. H., Xie, Z., Pesic, J., Sosnick, T. R. *et al.* (2008). A large collapsed-state RNA can exhibit simple exponential single-molecule dynamics. *J. Mol. Biol.* **378**, 943–953.
43. Zhuang, X. W., Bartley, L. E., Babcock, H. P., Russell, R., Ha, T. J., Herschlag, D. & Chu, S. (2000). A single-molecule study of RNA catalysis and folding. *Science*, **288**, 2048–2051.
44. Russell, R., Zhuang, X. W., Babcock, H. P., Millett, I. S., Doniach, S., Chu, S. & Herschlag, D. (2002). Exploring the folding landscape of a structured RNA. *Proc. Natl Acad. Sci. USA*, **99**, 155–160.
45. Bartley, L. E., Zhuang, X. W., Das, R., Chu, S. & Herschlag, D. (2003). Exploration of the transition state for tertiary structure formation between an RNA helix and a large structured RNA. *J. Mol. Biol.* **328**, 1011–1026.
46. Hohng, S., Wilson, T. J., Tan, E., Clegg, R. M., Lilley, D. M. J. & Ha, T. J. (2004). Conformational flexibility of four-way junctions in RNA. *J. Mol. Biol.* **336**, 69–79.
47. Kim, H. D., Nienhaus, G. U., Ha, T., Orr, J. W., Williamson, J. R. & Chu, S. (2002). Mg^{2+}-dependent conformational change of RNA studied by fluorescence correlation and FRET on immobilized single molecules. *Proc. Natl Acad. Sci. USA*, **99**, 4284–4289.
48. Steiner, M., Karunatilaka, K. S., Sigel, R. K. O. & Rueda, D. (2008). Single-molecule studies of group II intron ribozymes. *Proc. Natl Acad. Sci. USA*, **105**, 13853–13858.
49. Steiner, M., Rueda, D. & Sigel, R. K. O. (2009). Ca^{2+} induces the formation of two distinct subpopulations of group II intron molecules. *Angew. Chem., Int. Ed. Engl.* **48**, 9739–9742.
50. Greenleaf, W. J., Frieda, K. L., Foster, D. A. N., Woodside, M. T. & Block, S. M. (2008). Direct observation of hierarchical folding in single riboswitch aptamers. *Science*, **319**, 630–633.
51. Brion, P. & Westhof, E. (1997). Hierarchy and dynamics of RNA folding. *Annu. Rev. Biophys. Biomol. Struct.* **26**, 113–137.
52. Batey, R. T., Rambo, R. P. & Doudna, J. A. (1999). Tertiary motifs in RNA structure and folding. *Angew. Chem., Int. Ed. Engl.* **38**, 2327–2343.
53. Butcher, S. E. & Pyle, A. M. (2011). The molecular interactions that stabilize RNA tertiary structure: RNA motifs, patterns, and networks. *Acc. Chem. Res.* **44**, 1302–1311.
54. Costa, M. & Michel, F. (1995). Frequent use of the same tertiary motif by self-folding RNAs. *EMBO J.* **14**, 1276–1285.
55. Murphy, F. L. & Cech, T. R. (1994). GAAA tetraloop and conserved bulge stabilize tertiary structure of a group I intron domain. *J. Mol. Biol.* **236**, 49–63.
56. Massire, C., Jaeger, L. & Westhof, E. (1998). Derivation of the three-dimensional architecture of bacterial ribonuclease P RNAs from comparative sequence analysis. *J. Mol. Biol.* **279**, 773–793.
57. Tanner, M. A. & Cech, T. R. (1995). An important RNA tertiary interaction of group I and group II introns is implicated in Gram-positive RNase P RNAs. *RNA*, **1**, 349–350.
58. Butcher, S. E., Dieckmann, T. & Feigon, J. (1997). Solution structure of a GAAA tetraloop receptor RNA. *EMBO J.* **16**, 7490–7499.
59. Jucker, F. M. & Pardi, A. (1995). GNRA tetraloops make a U-turn. *RNA*, **1**, 219–222.
60. Davis, J. H., Tonelli, M., Scott, L. G., Jaeger, L., Williamson, J. R. & Butcher, S. E. (2005). RNA helical packing in solution: NMR structure of a 30 kDa GAAA tetraloop–receptor complex. *J. Mol. Biol.* **351**, 371–382.
61. Qin, P. Z., Butcher, S. E., Feigon, J. & Hubbell, W. L. (2001). Quantitative analysis of the isolated GAAA tetraloop/receptor interaction in solution: a site-directed spin labeling study. *Biochemistry*, **40**, 6929–6936.
62. Davis, J. H., Foster, T. R., Tonelli, M. & Butcher, S. E. (2007). Role of metal ions in the tetraloop–receptor complex as analyzed by NMR. *RNA*, **13**, 76–86.
63. Downey, C. D., Fiore, J. L., Stoddard, C. D., Hodak, J. H., Nesbitt, D. J. & Pardi, A. (2006). Metal ion dependence, thermodynamics, and kinetics for intramolecular docking of a GAAA tetraloop and receptor connected by a flexible linker. *Biochemistry*, **45**, 3664–3673.
64. Hodak, J. H., Downey, C. D., Fiore, J. L., Pardi, A. & Nesbitt, D. J. (2005). Docking kinetics and equilibrium of a GAAA tetraloop-receptor motif probed by single-molecule FRET. *Proc. Natl Acad. Sci. USA*, **102**, 10505–10510.
65. Fiore, J. L., Holmstrom, E. D. & Nesbitt, D. J. (2012). Entropic origin of Mg^{2+}-facilitated RNA folding. *Proc. Natl Acad. Sci. USA*, **109**, 2902–2907.
66. Vander Meulen, K. A. & Butcher, S. E. (2012). Characterization of the kinetic and thermodynamic landscape of RNA folding using a novel application of isothermal titration calorimetry. *Nucleic Acids Res.* **40**, 2140–2151.
67. Holmstrom, E. D., Fiore, J. L. & Nesbitt, D. J. (2012). Thermodynamic origins of monovalent-facilitated RNA folding. *Biochemistry*, **51**, 3732–3743.

68. Xie, Z., Srividya, N., Sosnick, T. R., Pan, T. & Scherer, N. F. (2004). Single-molecule studies highlight conformational heterogeneity in the early folding steps of a large ribozyme. *Proc. Natl Acad. Sci. USA*, **101**, 534–539.
69. Leipply, D. & Draper, D. E. (2010). Dependence of RNA tertiary structural stability on Mg^{2+} concentration: interpretation of the Hill equation and coefficient. *Biochemistry*, **49**, 1843–1853.
70. Takamoto, K., Das, R., He, Q., Doniach, S., Brenowitz, M., Herschlag, D. & Chance, M. R. (2004). Principles of RNA compaction: insights from the equilibrium folding pathway of the P4–P6 RNA domain in monovalent cations. *J. Mol. Biol.* **343**, 1195–1206.
71. Leipply, D., Lambert, D. & Draper, D. E. (2009). Ion–RNA interactions: thermodynamic analysis of the effects of mono- and divalent ions on RNA conformational equilibria. *Methods Enzymol.* **469**, 433–463.
72. Rook, M. S., Treiber, D. K. & Williamson, J. R. (1999). An optimal Mg^{2+} concentration for kinetic folding of the *Tetrahymena* ribozyme. *Proc. Natl Acad. Sci. USA*, **96**, 12471–12476.
73. Ditzler, M. A., Rueda, D., Mo, J. J., Hakansson, K. & Walter, N. G. (2008). A rugged free energy landscape separates multiple functional RNA folds throughout denaturation. *Nucleic Acids Res.* **36**, 7088–7099.
74. Solomatin, S. V., Greenfeld, M., Chu, S. & Herschlag, D. (2010). Multiple native states reveal persistent ruggedness of an RNA folding landscape. *Nature*, **463**, 681–686.
75. Koculi, E., Thirumalai, D. & Woodson, S. A. (2006). Counterion charge density determines the position and plasticity of RNA folding transition states. *J. Mol. Biol.* **359**, 446–454.
76. Ohtaki, H. & Radnai, T. (1993). Structure and dynamics of hydrated ions. *Chem. Rev.* **93**, 1157–1204.
77. Sakuma, H. & Kawamura, K. (2011). Structure and dynamics of water on Li^+-, Na^+-, K^+-, Cs^+-, H_3O^+-exchanged muscovite surfaces: a molecular dynamics study. *Geochim. Cosmochim. Acta*, **75**, 63–81.
78. Meek, D. W. & Ibers, J. A. (1970). Crystal structure of hexaamminecobalt(III) tetrachlorozincate(II) chloride, [Co(NH3)6][ZnCl4] Cl. *Inorg. Chem.* **9**, 465.
79. Koculi, E., Lee, N. K., Thirumalai, D. & Woodson, S. A. (2004). Folding of the *Tetrahymena* ribozyme by polyamines: importance of counterion valence and size. *J. Mol. Biol.* **341**, 27–36.
80. Manning, G. S. (1978). Molecular theory of polyelectrolyte solutions with applications to electrostatic properties of polynucleotides. *Q. Rev. Biophys.* **11**, 179–246.
81. Misra, V. K. & Draper, D. E. (1999). The interpretation of Mg^{2+} binding isotherms for nucleic acids using Poisson–Boltzmann theory. *J. Mol. Biol.* **294**, 1135–1147.
82. Dammertz, K., Hengesbach, M., Helm, M., Nienhaus, G. U. & Kobitski, A. Y. (2011). Single-molecule FRET studies of counterion effects on the free energy landscape of human mitochondrial lysine tRNA. *Biochemistry*, **50**, 3107–3115.
83. Record, M. T., Anderson, C. F. & Lohman, T. M. (1978). Thermodynamic analysis of ion effects on binding and conformational equilibria of proteins and nucleic acids: roles of ion association or release, screening, and ion effects on water activity. *Q. Rev. Biophys.* **11**, 103–178.
84. Record, M. T., Zhang, W. T. & Anderson, C. F. (1998). Analysis of effects of salts and uncharged solutes on protein and nucleic acid equilibria and processes: a practical guide to recognizing and interpreting polyelectrolyte effects, Hofmeister effects, and osmotic effects of salts. *Adv. Protein Chem.* **51**, 281–353.
85. Grilley, D., Soto, A. M. & Draper, D. E. (2006). Mg^{2+}–RNA interaction free energies and their relationship to the folding of RNA tertiary structures. *Proc. Natl Acad. Sci. U.S.A.* **103**, 14003–14008.
86. Lambert, D., Leipply, D., Shiman, R. & Draper, D. E. (2009). The influence of monovalent cation size on the stability of RNA tertiary structures. *J. Mol. Biol.* **390**, 791–804.
87. Zhou, H. X. (2010). Rate theories for biologists. *Q. Rev. Biophys.* **43**, 219–293.
88. Hanggi, P., Talkner, P. & Borkovec, M. (1990). Reaction-rate theory: 50 years after Kramers. *Rev. Mod. Phys.* **62**, 251–341.
89. Frauenfelder, H. & Wolynes, P. G. (1985). Rate theories and puzzles of heme protein kinetics. *Science*, **229**, 337–345.
90. Zhou, H. X. (2003). Theory for the rate of contact formation in a polymer chain with local conformational transitions. *J. Chem. Phys.* **118**, 2010–2015.
91. Silverman, S. K. & Cech, T. R. (2001). An early transition state for folding of the P4–P6 RNA domain. *RNA*, **7**, 161–166.
92. Seol, Y., Skinner, G. M., Visscher, K., Buhot, A. & Halperin, A. (2007). Stretching of homopolymeric RNA reveals single-stranded helices and base-stacking. *Phys. Rev. Lett.* **98**, 158103.
93. Dewey, T. G. & Turner, D. H. (1979). Laser temperature-jump study of stacking in adenylic acid polymers. *Biochemistry*, **18**, 5757–5762.
94. Chu, V. B., Lipfert, J., Bai, Y., Pande, V. S., Doniach, S. & Herschlag, D. (2009). Do conformational biases of simple helical junctions influence RNA folding stability and specificity? *RNA*, **15**, 2195–2205.
95. Nissen, P., Ippolito, J. A., Ban, N., Moore, P. B. & Steitz, T. A. (2001). RNA tertiary interactions in the large ribosomal subunit: the A-minor motif. *Proc. Natl Acad. Sci. USA*, **98**, 4899–4903.
96. Doherty, E. A., Batey, R. T., Masquida, B. & Doudna, J. A. (2001). A universal mode of helix packing in RNA. *Nat. Struct. Biol.* **8**, 339–343.
97. Bailor, M. H., Sun, X. Y. & Al-Hashimi, H. M. (2010). Topology links RNA secondary structure with global conformation, dynamics, and adaptation. *Science*, **327**, 202–206.
98. Klostermeier, D. & Millar, D. P. (2000). Helical junctions as determinants for RNA folding: origin of tertiary structure stability of the hairpin ribozyme. *Biochemistry*, **39**, 12970–12978.
99. Aitken, C. E., Marshall, R. A. & Puglisi, J. D. (2008). An oxygen scavenging system for improvement of dye stability in single-molecule fluorescence experiments. *Biophys. J.* **94**, 1826–1835.
100. Rasnik, I., McKinney, S. A. & Ha, T. (2006). Nonblinking and long-lasting single-molecule fluorescence imaging. *Nat. Methods*, **3**, 891–893.
101. Kimberly, M. M. & Goldstein, J. H. (1981). Determination of pK_a values and total proton distribution

pattern of spermidine by ^{13}C nuclear magnetic resonance titrations. *Anal. Chem.* **53**, 789–793.
102. Förster, T. (1948). Zwischen molekulare energie wanderung und fluoreszenz. *Ann. Phys.* **2**, 55–75.
103. Kuno, M., Fromm, D. P., Hamann, H. F., Gallagher, A. & Nesbitt, D. J. (2001). "On"/"off" fluorescence intermittency of single semiconductor quantum dots. *J. Chem. Phys.* **115**, 1028–1040.
104. McKinney, S. A., Joo, C. & Ha, T. (2006). Analysis of single-molecule FRET trajectories using hidden Markov modeling. *Biophys. J.* **91**, 1941–1951.
105. Fiore, J. L., Kraemer, B., Koberling, F., Erdmann, R. & Nesbitt, D. J. (2009). Enthalpy-driven RNA folding: single-molecule thermodynamics of tetraloop–receptor tertiary interaction. *Biochemistry*, **48**, 2550–2558.